Transient chaos induces anomalous transport properties of an underdamped Brownian particle

David Speer, Ralf Eichhorn, and Peter Reimann
Universität Bielefeld, Fakultät für Physik, 33615 Bielefeld, Germany
(Received 18 June 2007; published 12 November 2007)

For an underdamped Brownian particle in a one-dimensional periodic potential we theoretically predict three unusual transport properties: (i) A static bias force (of either sign) generates an average particle motion in the opposite direction. (ii) A small bias leads to a particle transport in the direction of the bias, but upon increasing the bias the particle velocity reverses direction. (iii) For a given bias force, the particle motion follows the direction of the force for low temperatures, but upon increasing the temperature reverses its direction. The considered model is shown to be minimal for the occurrence of these phenomena. A detailed analysis of its deterministic properties and the influence of thermal noise is carried out with numerical simulations that are complemented by analytical approximations. Intuitive explanations of the basic mechanism behind the three effects are provided; their origin is attributed to a subtle interplay between the stability of coexisting attractors, noise induced metastability, and transient chaos. An experimental system for the realization of the predicted effects is given within the Stewart-McCumber model for Josephson junctions. Suitable parameter values for which these effects can be observed are quite realistic experimentally.

DOI: 10.1103/PhysRevE.76.051110 PACS number(s): 05.40.−a, 05.45.−a, 05.60.−k

I. INTRODUCTION

The interplay of nonlinearity and (thermal) noise in nonequilibrium systems often gives rise to quite unusual emerging properties, in the sense that they might seem at first glance to contradict physical intuition or everyday experience. Prominent examples are the stabilization of transient chaos by noise [1,2], ratchet effects [3], stochastic resonance [4], enhancement of diffusion [5], and noise suppression by noise [6], to name but a few. In many cases, such unusual properties can be revealed by considering the "characteristics" of the system in the form of a response to an external perturbation.

Here, we predict three anomalous transport properties of a single Brownian particle in one dimension by studying its response to an external static bias force:

(i) In the absence of the bias the symmetry of the system rules out any systematic transport. When perturbing the system by a static force of either sign (but not too large modulus) the result is an average motion with velocity of just the opposite sign. This quite astonishing response behavior is referred to as "absolute negative mobility" (see [7] for a recent review). For single Brownian particles, it has been theoretically studied so far in two-dimensional structured systems [8] or by including an "internal" degree of freedom [9]. Experimentally, it has been observed for charged Brownian particles in structured microfluidic devices [10], and due to quantum effects in a sample of bulk GaAs [11] and in semiconductor heterostructures [12]. In the latter two cases one also speaks of "absolute negative conductance." For a more detailed account of the quite extensive literature (mainly theoretical) we refer to [7].

(ii) For small bias forces, the transport direction is as usual, i.e., in the direction of the bias. However, upon increasing the bias the transport velocity suddenly changes sign and switches to the direction opposite to the external force, before returning to normal for even larger bias forces. To our knowledge, such a paradoxical nonlinear response has so far only been reported in the theoretical studies [13] of single Brownian particles confined to two-dimensional meandering structures.

(iii) For a given bias force, the transport behavior is as usual for low temperatures, but upon raising the temperature, first turns anomalous and later again normal. In other words, by increasing the random fluctuations due to thermal noise the transport velocity can be reversed to be opposite to the bias, in contradiction to our intuitive expectation that an increase of noise would support the downhill motion in the direction of the bias.

With the present work we continue and provide the details of our brief account [14] on the existence of the above described transport phenomena (i)–(iii) in a one-dimensional dynamics of a Brownian particle for which inertial effects play a dominant role. An independent, closely related investigation of the above effect (i) has recently been published in Ref. [15]. While the qualitative findings therein agree with ours, the underlying physical mechanisms are fundamentally different in the two cases, as detailed in Sec. V D below. Moreover, our approach to analyze the observed effects is complementary to the one from Ref. [15], admitting additional insight into the underlying physical mechanisms.

The paper is organized as follows: In Sec. II we introduce our model and the observable of main interest, namely, the average particle velocity. In Sec. III basic properties of our model are discussed: It is shown that this model is minimal for the occurrence of the above described effects (i)–(iii), in particular, a no-go theorem is mathematically proven for the case of overdamped one-dimensional systems. Focusing on the above effect (i), Sec. IV contains a detailed analysis of the deterministic properties of the model. The observed chaotic behavior in the deep nonlinear regime does not admit a quantitative analytical treatment. Instead, numerical simulations are complemented by intuitive explanations of the basic physical mechanism behind the occurrence of absolute negative mobility. Noise effects due to finite temperatures are thoroughly discussed in Sec. V and analytical approximations for the average particle velocity are provided that agree

 ©2007 The American Physical Society

well with the numerical simulations. After this detailed analysis of absolute negative mobility, the occurrence of the other two phenomena (ii) and (iii) in our model follows quite naturally and is easily understood, as described in Sec. VI. In Sec. VII, Josephson junctions with the property that they can be well modeled by the so-called resistively and capacitively shunted junction (RCSJ) or Stewart-McCumber model are considered as a concrete experimental system to which our theoretical predictions apply. Suitable parameter values for which the effects (i)–(iii) can be observed are quite realistic experimentally. Finally, we conclude and discuss our results with Sec. VII.

II. MODEL

Our working model consists of the one-dimensional dynamics of a Brownian particle with coordinate $x(t)$, mass M, and friction coefficient η [16],

$$M\ddot{x}(t) = -\eta\dot{x}(t) - V'(x(t)) + f(t) + F + \sqrt{2\eta T}\xi(t), \quad (1)$$

where $V(x)=V(x+L)=V(-x)$ is a *spatially symmetric*, *L-periodic potential*, $f(t)=-f(t+\tau/2)$ is a *temporally symmetric*, *τ-periodic driving*, F is a dc bias, and thermal fluctuations are modeled as usual by unbiased, δ-correlated Gaussian noise $\xi(t)$ with units of the temperature T such that Boltzmann's constant equals one. Furthermore, we focus on the simplest example, namely, purely harmonic potentials $V(x)$ and drivings $f(t)$, and we adopt dimensionless units of time, length, and mass such that

$$M = 1, \quad V(x) = -\cos x, \quad f(t) = A\sin(\omega t), \quad (2)$$

i.e., $L=2\pi$ and $\tau=2\pi/\omega$. More general models will be briefly addressed at the end of the paper.

Driven Brownian motion in a periodic potential is of relevance in many different contexts, such as atomic friction, fluxons in semiconductors, superionic conductors, Josephson junctions, charge density waves, phase and mode locking phenomena, intracellular transport, neural activity, and so on (see, e.g., Refs. [16,17], and references therein). The corresponding minimal model (1) and (2) has been extensively studied, e.g., from the viewpoints of noisy chaos and phase locking [18–22], resonance activation [23,24], stochastic resonance [25], and escape processes [26–28]. An even much larger literature is available if one also includes slight modifications (e.g., nonharmonic V or f), generalizations (e.g., two-dimensional models), or special limits (vanishing M,η,T,f, etc.) of the basic model (1) and (2), addressing various aspects of ratchet effects [3(b),29,30] and diffusive transport [16,17], to name but two examples.

The observable of foremost interest in Eqs. (1) and (2) will be the time and ensemble averaged particle velocity

$$v := \frac{\tau}{L}\left\langle \lim_{t\to\infty}\frac{1}{t}\int_0^t dt'\dot{x}(t')\right\rangle, \quad (3)$$

expressed as a dimensionless multiple of the spatial and temporal periods L and τ. The ensemble average is indicated by $\langle\cdot\rangle$ and the time average ensures independence of initial transients and of the τ-periodic oscillations imposed by the driving $f(t)$ in Eq. (1).

III. BASIC PROPERTIES, MINIMAL MODEL, AND NO-GO THEOREM

The dynamics (1) and (2) is ergodic for any finite noise strength ηT and hence the velocity (3) unique (independent of initial conditions). For symmetry reasons, it follows that $F\mapsto -F$ implies $v\mapsto -v$, in particular, $v=0$ for $F=0$. As mentioned at the beginning, our main objective will be to find situations with opposite signs of F and v. To appreciate that such a behavior is indeed quite astonishing, we first give three arguments which—at first glance—seem to prohibit it altogether.

First, according to Newton's second law, when increasing the force from $F=0$ to a finite value one should always expect a finite acceleration in the same direction and hence a change of the velocity from $v=0$ to a finite value of the same sign. This argument, however, is no longer conclusive for a *nonlinear* dynamics: one cannot simply superimpose the effects of those forces which are already present when $F=0$ with the effect of an additional finite F. Indeed there is one nonlinear term in Eqs. (1) and (2), namely, $-V'(x)$.

Second, one might object that a velocity v opposite to a dc force F contradicts thermodynamic stability criteria, the principle of Le Châtelier, and ultimately the second law of thermodynamics. Again, such an argument is no longer conclusive for systems *out of equilibrium* [31]. The latter is guaranteed in Eq. (1) by the periodic driving $f(t)$.

Third, let us consider any one-dimensional stochastic dynamics of the form

$$\dot{x}(t) = h(x(t),t) + F + g(x(t),t)\xi(t), \quad (4)$$

whose solutions $x(t)$ are almost certainly ergodic and continuous. Furthermore, let us define v as in Eq. (3) but without the prefactor τ/L. For ergodicity reasons, the time average is equivalent to the ensemble average, hence the latter is in fact superfluous. It follows that $v=\lim_{t\to\infty}x(t)/t$, independent of $x(0)$ and independent of the particular realization of the noise $\xi(t)$ [3(b)]. Next, consider two solutions $x_1(t)$ and $x_2(t)$ of Eq. (4) with identical seeds $x_1(0)=x_2(0)$ and identical realizations of the noise $\xi(t)$, but with different dc bias F, say $F_1 > F_2$. Then, for any t with the property $x_1(t)=x_2(t)$ it follows from Eq. (4) that $\dot{x}_1(t)-\dot{x}_2(t)=F_1-F_2>0$. Exploiting continuity, we can infer that $x_1(t)\geqslant x_2(t)$ for all t and hence $v_1 \geqslant v_2$ [32]. In other words, v is a monotonically increasing function of F, implying the following *no-go theorem*: v and F cannot have opposite signs for any continuous, ergodic dynamics of the form (4) with $v=0$ for $F=0$. In a special case, namely, for t-independent h and constant g in Eq. (4), the same conclusion has been reached in a completely different way in Ref. [33]. For our purposes, the above generalization for t-dependent h in Eq. (4) is indispensable. Namely, by comparison with Eqs. (2) we now can rigorously rule out opposite signs of v and F in the absence of the *inertia term* $M\ddot{x}(t)$ in Eq. (1) (overdamped limit).

Omitting the *dissipative term* $-\eta\dot{x}(t)$ in Eq. (1) is equiva-

lent to the limit $\eta \to 0$ with ηT kept fixed, i.e., a system coupled to an infinitely hot bath. Then, the effect of the potential force $-V'(x(t))$ is negligible. As seen above, this excludes v opposite to F.

As we will see later, without the last term in Eq. (1), v opposite to F is still possible but this may now depend on the choice of the initial conditions. Apart from that, we can conclude that every single term in Eq. (1) is indispensable. In this sense *the model (1) and (2) is minimal*.

It remains to be shown that this minimal model indeed can give rise to net motion against the average force [34]. In general, the dynamics (1) and (2) exhibits an extremely rich behavior as a function of its parameters η, A, ω, F, T. A general overview is provided, e.g., by Refs. [20–22]. Our objective is not such a systematic exploration but rather to unravel the above mentioned anomalous transport behavior.

Such a behavior can readily be ruled out for very small and large frequencies ω: Below some lower limit an adiabatic approximation becomes valid [35], and beyond some upper limit an approximation by means of Bessel functions holds [22]; absolute negative mobility is ruled out within the range of validity of both approximations. Our detailed analysis shows that the lower limit is about 0.01, and the upper limit about 2, and that

$$\omega = 0.6 \tag{5}$$

is close to the optimal choice (see also the following discussion). Moreover, as already mentioned before, for large temperatures T the effects of the potential force $-V'(x)$ in Eq. (1) become negligible. The remaining linear dynamics (1) is readily solved, yielding for the velocity (3) the result

$$v \to \frac{\tau}{L}\frac{F}{\eta} \quad \text{for } T \to \infty \tag{6}$$

in the direction of F. Hence, we can focus on the low temperature regime.

IV. DETERMINISTIC BEHAVIOR

Starting with the unbiased dissipative dynamics (1) and (2) in the deterministic limit (i.e., $F=0$, $\eta>0$, $T=0$), the remaining control parameters are A and η. In general, analytical progress is still fairly hopeless [20–22], but numerical solutions are readily available. As usual [20–22,29], one finds that those deterministic solutions of the dissipative dynamics (1) and (2) either converge towards a periodic attractor [36] or maintain an aperiodic behavior in the long time limit, depending on the choice of A, η, and the initial conditions.

In the case of a periodic attractor, the resulting average velocity (3) is of the form $v=n/m$ with integers n and m, indicating that the periodic attractor proceeds by n spatial periods L of the potential $V(x)$ during m time periods τ of the driving $f(t)$ in Eq. (1). In the aperiodic case we distinguish between (i) phase locked aperiodic: the long time solution still proceeds by n elementary spatial cells during m time-periods, but with an aperiodic behavior of the reduced dynamics within the elementary cell $[0,L]$ [37], and (ii) non phase locked aperiodic [38].

A. Numerical findings

The colors in Fig. 1 summarize our numerical findings for a few dominating n/m ratios, including both periodic and phase locked aperiodic attractors. The remaining white regions refer to non phase locked attractors [39]. For symmetry reasons, every solution with $v \neq 0$ has a coexisting twin brother with opposite v. Further, v is invariant under $A \mapsto -A$. In agreement with what one would have expected, for very small and large amplitudes A, only solutions with $v=0$ survive. Also in agreement with the well known behavior in the Hamiltonian ($\eta \to 0$) and overdamped ($\eta \to \infty$) limits, for weak (but finite) dissipation η one typically finds a whole mess of coexisting attractors with different velocities v by probing different seeds [30], while for larger η the asymptotic velocity is in most cases unique apart from the above mentioned degeneracies due to symmetry [40]. Such a situation with unique velocity is, for instance, observed in the (η, A) regions around the two black crosses in Fig. 1, which indicate the parameter values we study in more detail below [see Eqs. (7) and (12)].

A magnification of the lowest red stripe in Fig. 1 is reproduced in Fig. 2(a), while in Figs. 2(b)–2(d) the effect of a finite static bias F in Eq. (1) is illustrated. As mentioned above, the red region in Fig. 2(a) comprises coexisting solutions for $F=0$ with either $v=1$ or $v=-1$. This degeneracy is lifted by gradually increasing F, and hence the regions with $v=1$ and $v=-1$ in Figs. 2(b)–2(d) start to diverge. Focusing on any point at the border of the colored region in Fig. 2(a) (an example is indicated by the larger black cross), there is a well defined local "speed" at which the two borderlines with $v=1$ and $v=-1$ in Figs. 2(b)–2(d) start to move apart upon increasing F. For any such border point (η, A) which turns blue in Figs. 2(b)–2(d) (e.g., the larger black cross) we thus expect a *velocity* $|v|=1$ *opposite to the static bias* F, at least for not too large $|F|$.

B. Basic physical mechanism

The way in which the two regions with $v=1$ and $v=-1$ in Fig. 2 move apart and deform upon variation of the bias F can be qualitatively understood by means of the following two intuitive arguments. First, it is quite clear that for sufficiently large F any net motion in the opposite direction will finally become impossible. This basically explains why the blue region in Fig. 2 shrinks and finally disappears upon increasing F, while the orange region grows (at least for not too large F; later it disappears as well). Second, it is plausible that for any fixed amplitude A, a solution with a given velocity $|v|=1$ will dissipate on average less energy when η is decreased. Now, consider any border point in Fig. 2(a) (e.g., the larger black cross) where the $|v|=1$ solutions cease to exist when η is decreased. But now, instead of decreasing η we apply a small positive bias $F>0$. Along the same lines, a solution with positive velocity $v=1$ gains energy on the average, which is basically equivalent to saying it dissipates less. Therefore we expect that this solution ceases to exist. While not rigorous, this argument explains why for any given A value the border under consideration moves into the direction of increasing η upon increasing F, at least for suf-

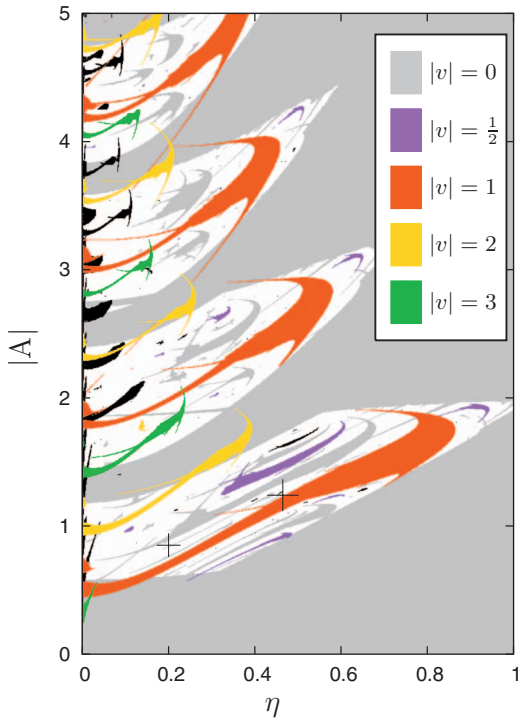

FIG. 1. (Color) Regions in the (η,A) plane with periodic and phase locked aperiodic attractors of the unbiased, deterministic, dissipative dynamics (1), (2), and (5), i.e., $F=0$, $T=0$, $\eta>0$, $\omega=0.6$, obtained by numerical integration sampling many different initial conditions. Colors: average velocity v from Eq. (3) on these attractors for a few dominating rational v values. Black: other rational v values. White: no phase locked attractors have been found. Overlapping of regions with different colors typically indicates coexistence of attractors. The larger black cross represents Eq. (7) and the smaller one Eq. (12).

ficiently small F (later, nonlinear corrections take over). Analogous arguments hold for any border point of the orange and blue regions in Fig. 2, thus explaining why they move to the right and left, respectively, upon increasing F. By inspection of Fig. 2, one furthermore sees that the parameter choice indicated by the larger black cross, i.e.,

$$\eta = 0.465, \quad A = 1.24, \tag{7}$$

is optimal in the sense that it remains within the blue region for the largest interval of F values.

C. Bifurcation diagrams

A more detailed illustration of the above reasoning is provided by Fig. 3. The panels (a)–(d) correspond to horizontal sections through the larger black cross in the corresponding panel of Fig. 2. The red dots in Figs. 3(a)–3(d) are a common way of visualizing attractors of a nonlinear dynamics [22]. These bifurcation diagrams reveal the two qualitatively different dynamical situations already classified above. The vertical red stripes that cover the whole spatial period L correspond to non phase locked aperiodic attractors, whereas the period-doubling cascades to chaos and the periodic windows comprise phase locked aperiodic and periodic attractors.

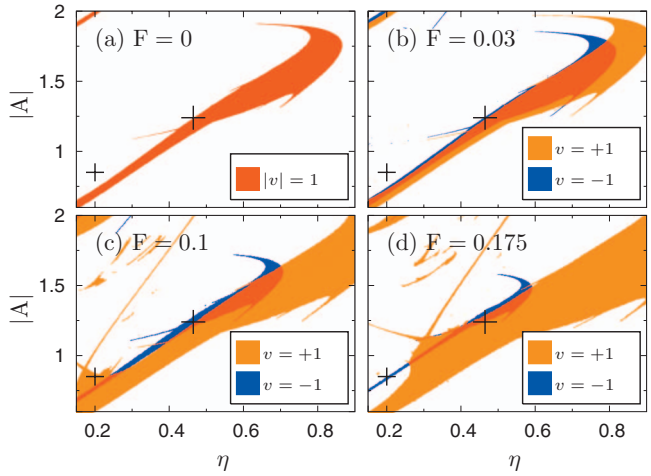

FIG. 2. (Color) (a) Magnification of the lowest red stripe in Fig. 1. The large black cross represents Eq. (7) and the small one represents Eq. (12). [(b)–(d)] Same except for $F>0$. Periodic and phase locked aperiodic attractors with $v=1$ are indicated in orange and those with $v=-1$ are indicated in blue, yielding red in the coexistence regions. Apart from this degeneracy due to symmetry (see also main text), the asymptotic velocities $v=\pm 1$ are unique, i.e., independent of initial conditions [39].

The large window without non phase locked aperiodic attractors in each panel corresponds to the colored region along the horizontal sections in Figs. 2(a)–2(d). Focusing on Fig. 3(a), we find $v=0$ in the entire non phase locked regime and within most of the small periodic windows. Within the large window, the phase locked solution with velocity $v=1$ and its symmetry partner with $v=-1$ are each generated by two attractors. All four attractors are born out of tangent bifurcations, coexist in a small η range around $\eta\approx 0.53$ (in which they are connected by an unstable invariant set in phase space), and are destroyed by way of crisis [22,41] after evolving through a period-doubling route to chaos. In particular, four phase-locked attractors coexist around $\eta\approx 0.53$, but only two velocities $v=1$ and $v=-1$ are observed. Note that in the stroboscopic map in Fig. 3(a) the actual symmetry of the $v=1$ and $v=-1$ solutions would be recovered after shifting the stroboscopic times for one of them by $\tau/2$.

For $F>0$ [Figs. 3(b)–3(d)] the symmetry of the period-doubling cascades is broken, especially their birth (tangent bifurcations) and death (crises) points along the η axis no longer coincide. As a consequence, a gap is opening up at the lower end of the phase locked regime (small η values), where only solutions with $v=-1$ remain possible, whereas the formerly coexisting solution with $v=1$ has lost stability and turned into a chaotic repeller [1]. An analogous gap opens up at the upper crises. Since one is dealing with either a periodic attractor or phase locked aperiodic solutions within the entire phase locked regime, structural stability implies that the time- and space-periodicities n and m do not change and hence the velocities $v=n/m$ indeed keep their values ± 1 upon changing F. In contrast, the velocity v within the η regimes with non phase locked aperiodic attractors is expected to depend continuously on the bias F and hence, in general, no longer vanishes for finite F.

The situation within the small windows is analogous to that in the large one, but beyond the resolution of Fig. 3. A

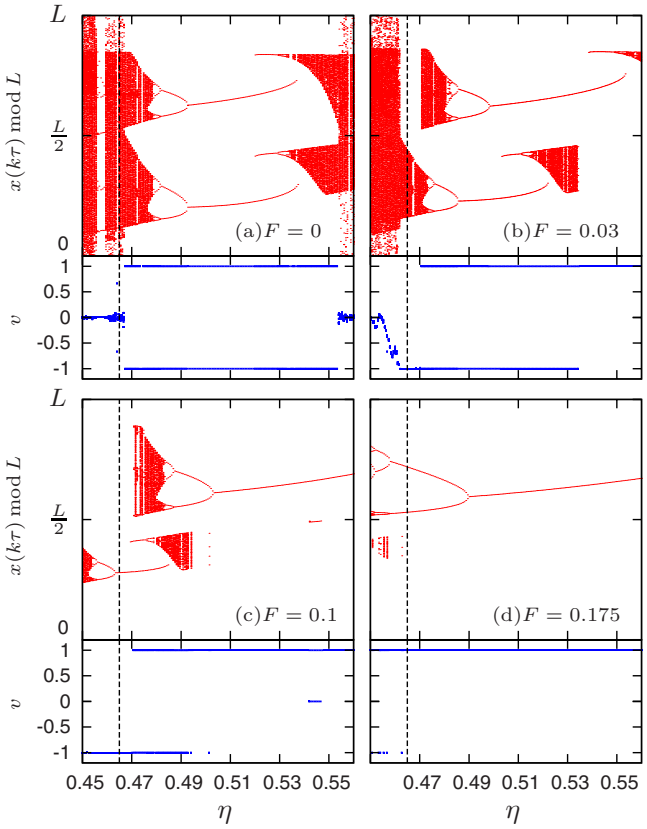

FIG. 3. (Color online) Bifurcation diagrams of attractors (red) [36] and concomitant velocities (blue) versus damping strength η from numerical solutions of the deterministic dissipative dynamics (1)–(3) with $T=0$, $\omega=0.6$, $A=1.24$ and the same values of the static bias F as in Fig. 2. For any given η and F, the red dots represent $x(k\tau)$ modulo L (stroboscopic map of the reduced spatial dynamics) for a set of sufficiently large integers k such that initial transients have died out. The dashed line at $\eta=0.465$ corresponds to the larger black cross in Fig. 2. Coexistence of different velocities v implies coexistence of attractors, but not vice versa.

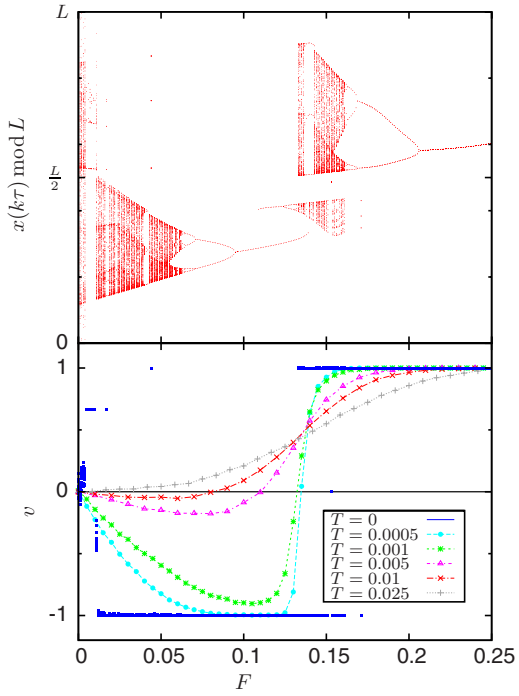

FIG. 4. (Color online) Same as Fig. 3(a), but keeping $\eta=0.465$ fixed and instead varying F. In addition, the numerically determined velocity v from Eq. (3) for various T is indicated in the lower part. The numerical uncertainty is of the order of the symbol size. The connecting lines serve as guides to the eye. Since $F \mapsto -F$ implies $v \mapsto -v$, negative F are omitted.

very small periodic window containing $v=\pm 2/3$ phase locked attractors is located in Fig. 3(a) at $\eta \approx 0.464$ just left to the dashed line, but is beyond the resolution of Fig. 3(a). It gives rise to another anomalous transport behavior as detailed in Sec. VI.

In the same vein, the results for $T=0$ in Fig. 4 can be readily understood by observing that they basically amount to a cut through Figs. 3(a)–3(d) along the dashed line (fixed $\eta=0.465$). The fact that the parameters in Eq. (7) do not exactly hit the borderline in Fig. 2(a) [see also Fig. 3(a)] explains why v does not immediately jump to -1 for $F>0$. A nice illustration of three coexisting attractors but only two velocities $v=1$ and $v=-1$ is visible around $F=0.13$ in Fig. 4.

According to our above explanations of Figs. 2–4, the simplest case of net motion opposite to the bias F is exemplified by the specific parameter choice (7) and $F=0.1$. In this case, there is a unique attractor of the deterministic dynamics (1), (2), and (5), consisting of a period $m=1$ orbit whose time evolution is illustrated by the nine snapshots in Fig. 5. Apparently, the delicately tuned up and down tilting of the total potential prevents the particle from running downhill and even stabilizes the periodic uphill motion against arbitrary perturbations of finite duration.

Basically, the solution in Fig. 5 advances by one spatial period during the first half time period and remains within the same spatial period in the second half time period. The same rough behavior applies for all the solutions within the lowest red stripe in Fig. 1. Likewise, the solutions within the next red stripe in Fig. 1 advance by two spatial periods during one half time period and then move back by one spatial period during the second half time period, and so on: in each red stripe the solutions advance by n and then return by $n-1$ spatial periods, resulting in $|v|=1$ in all cases, and similarly for the other colored stripes in Fig. 1.

Besides the "main" stripe of the lowest red region in Fig. 1 there are many very fine additional filaments emanating from this main stripe [see also Fig. 2(a)] (the one to the lower left of the larger black cross is relatively well visible; most of the others are at or below the resolution of the numerics or the figures). With increasing F the corresponding orange filaments in Fig. 2 start to grow and move somewhat. Some of the small periodic windows in Figs. 3 and 4 can be traced back to such filaments. If a filament crosses a part of one of the other main stripes with a different color in Fig. 1, there are several coexisting $|v|$ values. As announced above, the measure of parameter values (η, A) for which this is the case, is quite small for moderate-to-large η. Moreover, only the solutions within the main stripes are reasonably robust against parameter changes and perturbations, e.g., by weak noise.

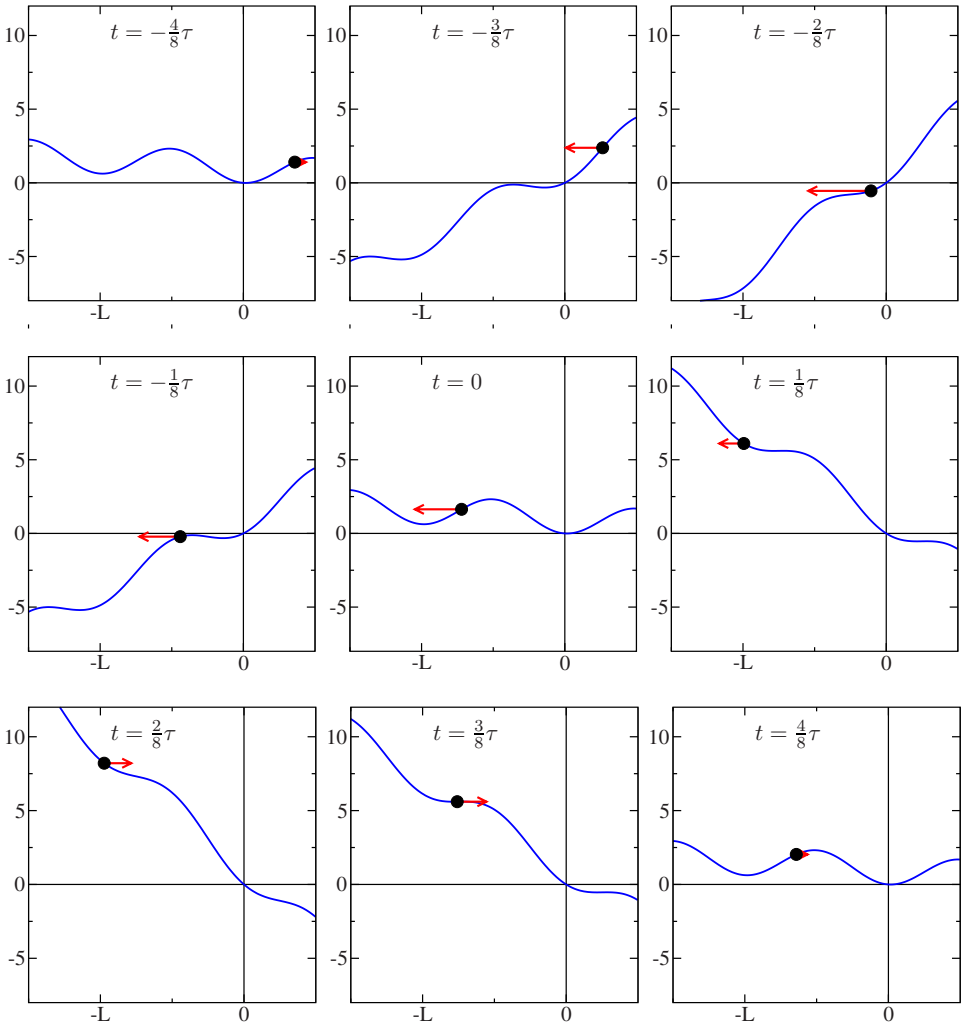

FIG. 5. (Color online) Time evolution of the unique attractor of the deterministic dynamics (1) and (2) with $T=0$, $\omega=0.6$, $A=1.24$, $\eta=0.465$ [cf. Eqs. (5) and (7)], and $F=0.1$. The black dots and red arrows indicate position and velocity of the stable period-one orbit $x(t)$ at nine time instances during one driving period. The blue curves represent the instantaneous total potential $V(x)-x[f(t)+F]+1$ according to Eqs. (1) and (2).

V. NOISE EFFECTS

Next we address the effect of thermal noise with finite temperatures T in Eq. (1). As mentioned at the end of Sec. III, we can focus on small T. The first main consequence of any finite T is that any deterministic attractor turns metastable, and due to the noise induced transitions between them the dynamics is always ergodic and hence the velocity (3) is independent of the initial condition. While in the deterministic case the unstable periodic orbits and chaotic repellers play no role with respect to the velocity (3), in the presence of noise they are back in the game during the transitions between the attractors. Essentially, the velocity (3) will thus be the average over the individual velocities of all the attractors and repellers, weighted according to their "lifetimes" [42].

To illustrate these qualitative arguments in more detail, we next compare numerical results for finite T step by step with our above findings for $T=0$. Figure 6 is the analog of Fig. 1 but for finite temperature T and bias F [43]. Apparently, the periodic and phase locked aperiodic solutions with $v=0$ (gray in Fig. 1) are quite robust against some noise and bias (white in Fig. 6). For the periodic and phase locked aperiodic solutions with finite v (colored in Fig. 1) the symmetry breaking $F>0$ in most cases leads to a dominance of the solutions with positive v (orange in Figs. 2 and 6) but also substantial regions with v opposite to F (blue in Figs. 2 and 6) survive at the upper borders of some colored stripes in Fig. 1. The quite notable positive velocities v within the lowest stripe in Fig. 6 and the negative velocities at the upper border of this stripe are obviously the noisy traces of the orange and blue regions in Fig. 2(c), and similarly for the other stripes in Fig. 6.

The main conclusion from Fig. 6 is that net motion against the bias F indeed can survive in the presence of noise. In fact, for any given friction η between 0.1 and 0.65 there exists an interval of amplitudes A with significant v opposite to F according to Fig. 6. Furthermore, comparison of the blue islands in Fig. 6 suggests that there are parameter values (η,A) whose motion against F is even somewhat faster and more robust than the one indicated by the larger black cross, however, with a more complicated deterministic motion than the one in Fig. 5. Its actual quantitative robustness against bias and noise is shown in Figs. 4 and 7. Hence, we expect that by optimizing parameters, one may be able to further improve the maximal F in Fig. 4 and the maximal T in Fig. 7 with v opposite to F (see Sec. V B below). A comparison of Figs. 1 and 6 furthermore suggests that periodic attractors of low period are more stable against noise than those of high period and phase locked aperiodic solutions.

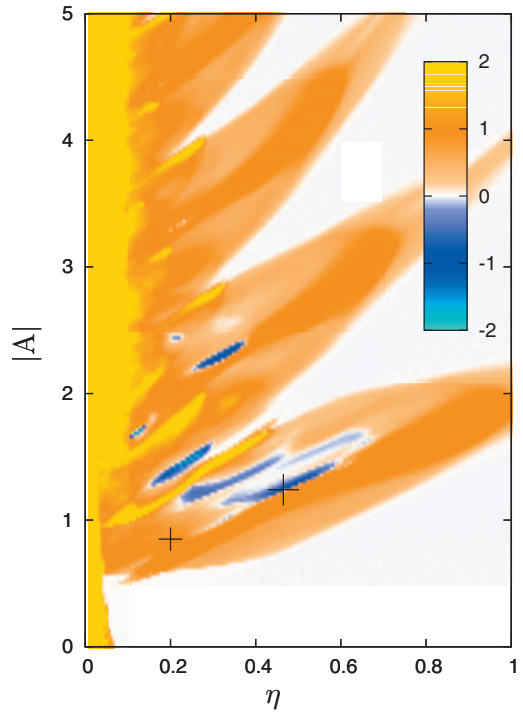

FIG. 6. (Color) Same as Fig. 1 but for $T=0.001$ and $F=0.1$. The value of the velocity v from Eq. (3) is independent of initial conditions and indicated by the coloring.

A. Analytic approximation

The noisy counterpart of the deterministic, period-one solution from Fig. 5 is depicted in Fig. 8. According to Fig. 8(a), roughly speaking, the trajectory seems to switch randomly between pieces with a negative slope v_- and pieces with a positive slope v_+. Those with v_- are almost perfectly periodic and indeed practically coincide with the deterministic period-one orbit and hence one readily understands that $v_-=-1$. Those with v_+ have an aperiodic fine structure which

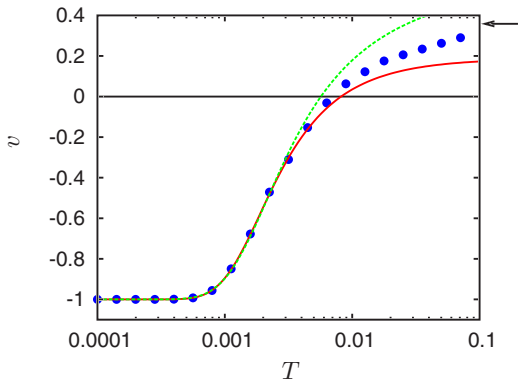

FIG. 7. (Color online) Symbols: Average velocity v from Eq. (3) versus temperature T from numerical solutions of Eqs. (1), (2), and (5) with parameter values (7) (labeled by the larger black cross in Figs. 1, 2, and 6) and with bias $F=0.1$. The numerical uncertainty is smaller than the symbol size. Red solid line: analytic approximation (8), (10), and (11); green dashed line: analytic approximation (9)–(11), with velocities $v_+=0.88$ and $v_-=-1$, cf. Fig. 9. Arrow: analytical asymptotics $v\to 0.358$ for $T\to\infty$ according to Eq. (6).

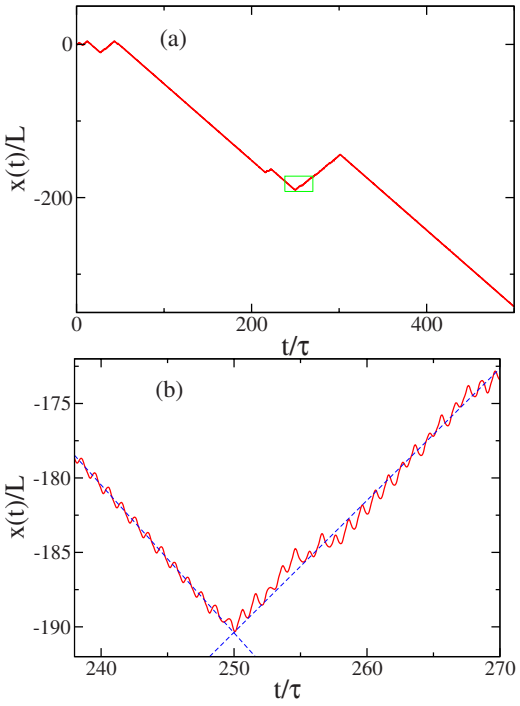

FIG. 8. (Color online) Typical numerical solution $x(t)$ of the dynamics (1), (2), and (5), with parameter values (7) (labeled by the larger black cross in Figs. 1, 2, and 6) and with $T=0.001$ and $F=0.1$. (a) Global behavior. (b) Magnification of the green window in (a). Dashed: straight lines with slopes $v_+=0.88$ and $v_-=-1$.

can be naturally understood as the fingerprint of the underlying chaotic repeller (see the above discussion of Fig. 3). Contrary to the naive first guess $v_+\approx 1$, the average velocity of long lived transients on the repeller is found to be $v_+\approx 0.88$ [cf. Fig. 8(b)]. In other words, the chaotic repeller does not strictly maintain the velocity of the former attractor, and in fact there does not seem to be any reason why it should do so.

We have analyzed the above noisy transitions between the period-one attractor and the chaotic repeller by extensive numerical simulations for a number of temperatures T between 2.5×10^{-3} and 6.7×10^{-4}. We found that they can be described very well in terms of escape rates k_- and k_+ from the periodic orbit and the repeller, respectively [42]. Thus, we adopt a two state Markov model for the system with the states being the attractor ("−" state) and the repeller ("+" state). Asymptotically, the escape rates are given by the inverse lifetimes of the states. In principle, these could be determined from the average (temporal) length of the uninterrupted $v=-1$ ($v\approx 0.88$, respectively) segments of the noisy trajectory (cf. Fig. 8). The length of these segments is expected to follow an exponential distribution for sufficiently long segments, and the average lifetimes can be obtained from the exponents of the cumulative distribution functions. However, the numerical determination of the time instant at which the motion switches from one state to the other turned out to be ambiguous when based only on the particle position $x(t)$. It is more convenient to use a well-defined set in the (x,v) phase space that represents the "−" state with motion on or close to the phase locked attractor, and to track when

the trajectory leaves this set and enters its complement, corresponding to the "+" state on the repeller.

This approach is illustrated with Fig. 9. The crosses represent the stroboscopic signature of the $v=-1$ attractor for three successive driving periods, i.e., if the trajectory starts on the rightmost cross in Fig. 9, it is located on the middle cross one period later, and on the left cross another period later. A deterministic solution ($T=0$) starting from any other point in the phase plane [44] (irrespective of its color) is eventually attracted to this periodic trajectory. The colored regions consist of those trajectories in phase space that, while converging to the attractor, move "synchronously" with a trajectory on that attractor, i.e., a point from the blue region jumps to the green region and then to the red region during two successive driving periods. We term this subset of the total basin of attraction the "synchronous basin of attraction," and use it to define the set in phase space that represents the "−" state of the noisy dynamics in the following way. A noisy trajectory switches from the "+" state to the "−" state when entering the blue part of the synchronous basin of attraction within the rightmost spatial period of Fig. 9 (or the green part within the middle period, or the red part within the left period, etc.), and remains in the "−" state until it leaves the synchronous basin of attraction of the associated attractor [22]. Consequently, a trajectory in the "−" state moves uphill against the force $F>0$ with $v=-1$ exactly like a trajectory on that attractor (and would continue to do so if the noise source is switched off). The behavior in the complementary "+" state is characterized by a downhill motion close to the chaotic repeller resulting in $v\approx 0.88$.

Based on this definition of the "+" and "−" states, the average lifetime of the attractor is calculated from the average time it takes a trajectory, initialized on the attractor [45], to leave the synchronous basin of attraction for the first time. The average lifetime of the repeller is determined from an ensemble method [1], which basically estimates the exponential part of the decay into the "−" state of a population of trajectories being initialized close to the repeller in the "+" state.

The temperature dependence of the resulting escape rates is shown in Fig. 10. The escape rate k_- from the attractor (red squares) is found to be well described by an Arrhenius law [22], whereas the escape rate k_+ from the repeller (blue dots) is found to be roughly temperature independent (cf. solid lines in Fig. 10)

$$k_- = 0.14\exp(-0.0034/T), \quad k_+ = 0.081. \tag{8}$$

These approximations can be improved by taking into account the temperature dependence of the prefactor in the Arrhenius law of k_- [46], and by heuristically including a lowest order temperature dependence of k_+ of the form $\sqrt{T}$, yielding (cf. dashed lines in Fig. 10).

$$k_- = 2.5\sqrt{T}\exp(-0.0028/T), \quad k_+ = 0.07 + 0.46\sqrt{T}. \tag{9}$$

Both, the Arrhenius form of k_- and the approximate T independence of k_+ are quite plausible, while the quantitative details are clearly beyond the analytical realm.

Next, the probabilities p_- and p_+ to be in the "−" state on the attractor and the "+" state on the repeller, respectively, will be approximately proportional to the inverse escape rates (lifetimes) and normalized, i.e.,

$$p_\pm = \frac{k_\pm^{-1}}{k_+^{-1} + k_-^{-1}}. \tag{10}$$

Finally, this suggests that one can approximate the velocity v by the average over the velocities $v_\pm$ associated with attractor and repeller, weighted with the respective probabilities $p_\pm$,

$$v \simeq v_+ p_+ + v_- p_-. \tag{11}$$

The agreement with the numerical results in Fig. 7 is remarkably good even at rather high T, where the rate theory is expected to fail. Surprisingly, the more sophisticated form (9) of the escape rates shows no notable improvement as compared to the less precise representation (8). The reason is that by Eq. (8) both, k_- and k_+, are underestimated for larger T (see Fig. 10) so that the respective errors compensate in Eq. (10).

B. Maximal temperature and bias

Next, we address the question: What is the maximally achievable temperature which still supports net motion against the applied bias, and similarly, what is the maximally achievable bias?

Figure 7 shows that the attracting properties of the periodic $v=-1$ orbit are overruled by thermal noise effects if T becomes large, so that finally the average velocity is in the direction of the bias F. Although it is clear from the discussion of Eq. (6) that for high enough temperatures T transport is always [i.e., for any values of the other parameters in Eq. (1)] in the direction of F, the quantitative details of the temperature region with v opposite to F depend on the specific properties of all attractors and repellers present, and thus on the specific parameter values in Eqs. (1) and (2). For our choice [Eq. (7)], e.g., we see from Fig. 4 (lower part) that a smaller bias F (still $F>0$) allows for larger T with an average motion against the bias. A more comprehensive picture of this observation is presented with Fig. 11, showing that part of Fig. 6, which contains the blue regions with average velocities opposite to F, for smaller bias but larger temperatures. From Fig. 11(d) we see that transport against the bias is possible even for temperatures as high as $T=0.04$ for optimized values of η and A.

One might conjecture that the temperature range with v opposite to F becomes largest for $F\to 0$. This is, however, not generally true, because the stability of the present attractors can change considerably with decreasing F, and even new attractors or repellers with other T-specific properties can come into play and dominate the transport behavior. Indeed the parameter values (7) constitute an example for such a situation, as discussed in detail in Sec. VI below.

From a complementary point of view, we may expect that the strength of the bias F at which the negative average velocity finally becomes positive and then follows the direction of F can be larger for smaller temperatures T. Although we could find (numerically) transport against the bias for forces up to $F=0.32$ at $T=4\times 10^{-5}$, a general statement is not possible in the same sense as above.

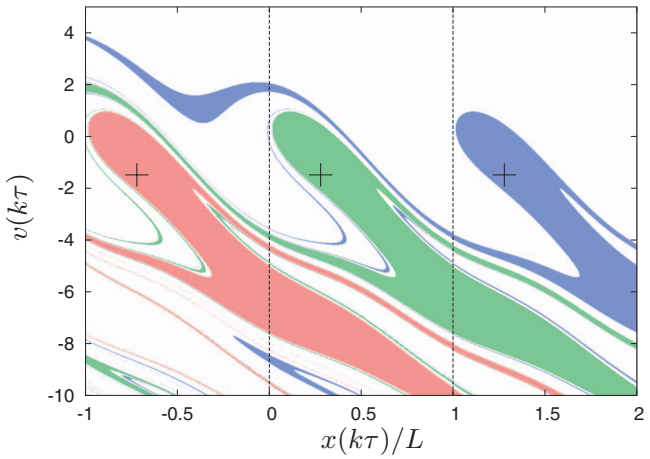

FIG. 9. (Color) Stroboscopic representation of the phase locked periodic attractor with $v=-1$ (black crosses), whose time evolution is illustrated in Fig. 5, shown within three spatial periods of the full (x,v) phase space (indicated by the dashed lines) for three consecutive driving periods. The colored regions represent the synchronous basin of attraction of the attractor (see main text) also for these three driving periods. The right cross and blue region correspond to the first, the middle cross and green region correspond to the second, and the left cross and red region correspond to the third driving period. This picture can be periodically repeated to the right and to the left to obtain the attractor and its synchronous basin of attraction for previous and later driving periods, respectively. The synchronous basins of attraction of all these periods have filaments that extend into the shown part of the phase space, and if one included them, they would completely cover the white region.

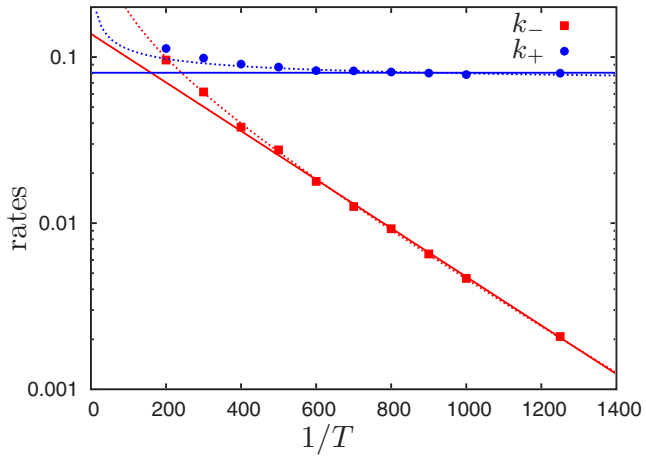

FIG. 10. (Color online) Arrhenius plot of the escape rates k_- and k_+ from the attractor (red squares) and the repeller (blue dots), respectively. Remaining parameter values: same as in Figs. 5 and 7–9. The statistical uncertainties are of the order of the symbol sizes. The solid lines represent the data fits (8); the dashed lines show Eq. (9). All fits are based only on the escape rates for temperatures $T \lesssim 0.0025$, because in this temperature range the description of the noisy trajectories in terms of transitions between the "+" and "−" state with respective escape rates k_+ and k_- is expected to be valid, as is self-consistently concluded from the obtained values in the exponents of Eqs. (8) and (9).

C. Speedy uphill motion

In comparison with purely noise-induced negative mobilities as studied in [7–9,13,15], the maximal velocities against the external bias observed here are considerably larger (typically at least by one order of magnitude). As detailed above, this is due to the fact that for not too large temperatures the noisy dynamics (1) is governed by the presence of phase locked attractors with deterministic transport in the direction opposite to the bias. Accordingly, the effect can readily be accelerated by exploiting phase locked attractors with higher velocities $|v|$ (see Fig. 1). As an example, we consider $n/m=3$ by choosing the parameter values given in Fig. 12. These values are located at the upper border of the green region in Fig. 1 around $\eta \approx 0,\ldots,0.23$ and $A \approx 1.5,\ldots,1.8$, which indicates the existence of a symmetric pair of period-one attractors with $|v|=3$. Hence, transport against the bias F occurs by the same mechanism as illustrated with Fig. 2 for the

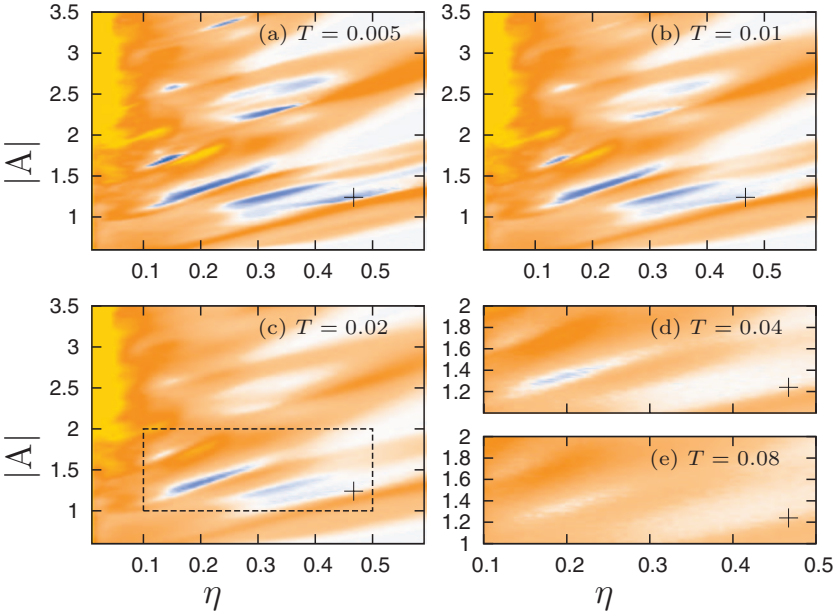

FIG. 11. (Color) Same as Fig. 6, but for $F=0.05$ and various T; blue indicates negative velocities with transport against the bias (see color panel in Fig. 6). (d) and (e) represent magnifications of the dashed box in (c), but for higher temperatures. Negative average velocities can still be observed for $T=0.04$. The black cross represents the parameter values (7).

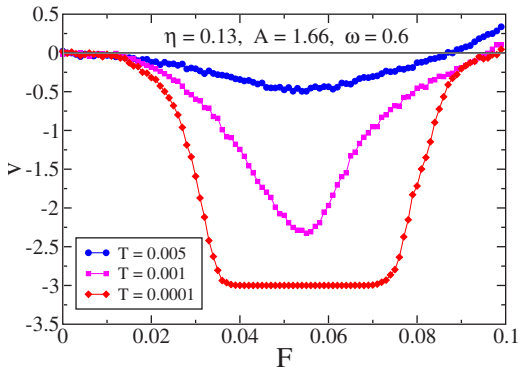

FIG. 12. (Color online) Average velocity v for the given parameter values and for various temperatures, obtained from numerical simulations of Eqs. (1) and (2). The indicated values for η and A are located at the upper border of a green region in Fig. 1 with deterministic transport velocities $|v|=3$.

$|v|=1$ attractors. The resulting speedy uphill motion is depicted in Fig. 12 for various temperatures T. Surprisingly, it is comparably robust against noise and only a little less stable with respect to increasing bias forces F as the slower uphill motion in Fig. 7.

In principle, unlimited acceleration of the uphill transport seems to be possible by using attractors with even higher deterministic velocities $|v|$. In practice, however, this is limited by the fact that such attractors are typically located at smaller η values in coexistence with other attractors, and only exist in rather small parameter regions.

D. Nontransporting attractors and comparison with Ref. [15]

Nontransporting phase locked deterministic solutions with $v=0$ typically exist over large parameter ranges (see, e.g., the gray region in Fig. 1). If there is a parameter region, in which such a nontransporting solution coexists with a symmetric pair of transporting attractors at $F=0$, then absolute negative mobility can occur for suitable parameter values at the border of that region by the same mechanism as detailed in Fig. 2. The only qualitative difference to Fig. 2 is that the white background would be gray, indicating the coexisting $v=0$ attractor. This situation is exemplified by Fig. 13 for some finite bias $F>0$ [compare to Fig. 2(c)]; suitable parameter values are located in the blue region, indicating the existence of a transporting attractor with $v=-1/2$. Correspondingly, the noisy trajectories at small temperatures T switch between three different states, since the uphill and downhill transporting "−" and "+" states are now complemented by a nontransporting "0" state. As a main consequence, the achievable velocities v opposite to F are slowed down considerably.

In contrast to the above situation, the parameter values indicated by the black cross in Fig. 13 are never reached by the blue region for any bias $F>0$ (nor by the orange and red regions). Nevertheless, absolute negative mobility can occur by another, different mechanism: Obviously, at $T=0$ we find $v=0$, because the nontransporting solution is globally attractive. At small temperatures T, however, the dynamics is governed not only by the stable $v=0$ orbit but also by two repellers that emerge from the $v=-1/2$ and $v=1/2$ attractors due to crises occurring at the borderlines of their stability regions (the blue and orange region in Fig. 13). Since the escape time from a repeller scales with the distance from the crisis according to some power law [47], and since the black cross in Fig. 13 for $F>0$ is closer to the blue than to the orange region, the major contribution of the chaotic repellers to the noisy trajectories comes from the repeller with negative $v\approx-1/2$. As a result, an average velocity v opposite to the bias F is observed for small temperatures T.

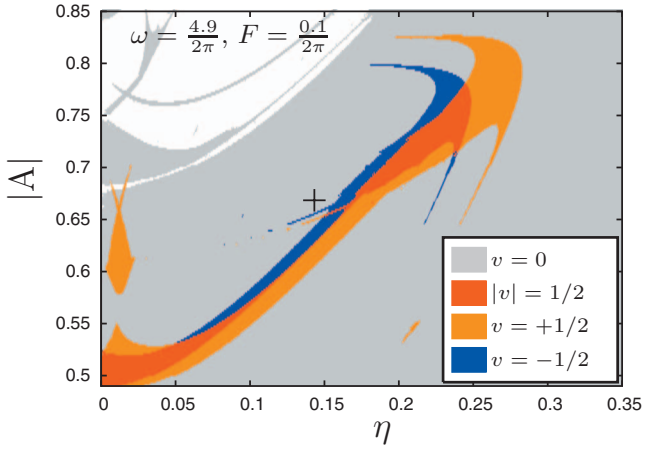

FIG. 13. (Color) Same as Fig. 2, but for the case of coexisting $v=0$ and $v=\pm\frac{1}{2}$ attractors. The indicated cross and the chosen frequency ω and bias force F represent the parameter values used in Figs. 1 and 2 of Ref. [15]; a vertical section through the cross corresponds to Fig. 1(a) therein. (Note that the units used by us and in Ref. [15] differ by some factors of 2π.)

The above explanations represent our announced complementary intuitive insight into the basic physical mechanism behind the effect of "absolute negative mobility induced by thermal equilibrium fluctuations," recently reported by Machura *et al.* [15]. While the latter effect *per se* is qualitatively very similar to the one discussed in the previous section of our present paper (see also Ref. [14] and footnote 22 in Ref. [15]), the underlying basic physical mechanism is thus quite different. Moreover, qualitatively the maximally achievable velocities are substantially smaller: In our units, the maximal velocity v opposite to a negative bias F reported by Machura *et al.* [15] is about $v=0.017$, and our more detailed numerical analysis of the parameter range from Fig. 13 indicates that one indeed can hardly do better.

In summary, the distinct feature of the effect reported in Ref. [15] is that it is purely noise induced, while the effect at the main focus of Ref. [14] and our present study has the advantage of producing much larger velocities.

VI. FURTHER ANOMALOUS TRANSPORT PROPERTIES

Our understanding so far of the system (1) and (2) allows us to readily predict further remarkable transport properties. Two examples are discussed in the following.

First, we consider the small black cross in Fig. 2 at

$$\eta=0.2, \quad A=0.85. \tag{12}$$

For small bias F we are somewhere in the white or gray domains of Fig. 1. Around $F=0.1$ the small black cross in

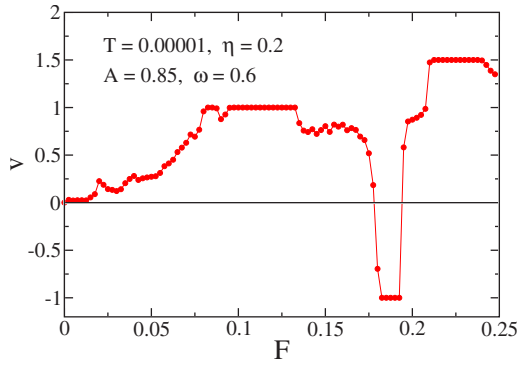

FIG. 14. (Color online) Symbols: Numerically determined velocity v from Eq. (3) for Eqs. (1) and (2) with parameters as indicated in the plot. The numerical uncertainty is smaller than the symbol size. The red line is a guide to the eye.

Fig. 2(c) penetrates a bulge of the orange area, which is "moving upwards" as a function of F. Hence, a velocity v of the same sign as F is expected. At the still larger F value in Fig. 2(d), the small black cross has left the orange bulge again and now instead is hit by the blue stripe, so that we expect a velocity v opposite to F. The corresponding prediction for the velocity v as a function of the bias F is nicely confirmed by the numerical simulations in Fig. 14. For small bias, the velocity direction is as usual, but changes sign upon increasing the bias, before returning to normal for even larger F [48].

Second, we focus on the small periodic window around $F=0.007$ in Fig. 4. This window represents an attractor with a unique deterministic velocity $v=2/3$ in the direction of the bias F. The reason for the appearance of this attractor at small bias forces is that the parameter values (7) indicated by the larger black cross in Fig. 1 are not exactly located at the upper border of the red stripe but somewhat above. The $v=-1$ attractor contained in this red region and emerging from it in blue in Fig. 2 reaches the larger black cross only at $F\approx 0.012$ (cf. Fig. 4); for smaller F it turns into a chaotic repeller. Similarly as in Eqs. (8)–(11), one thus has a competition between the deterministic attractor with $v_+=2/3$ and this chaotic repeller with $v_-\approx -1$. As confirmed by Fig. 15, for small T the attractor with $v\simeq 2/3$ wins, then the repeller with $v\simeq -1$ takes over, and finally, the usual large-T

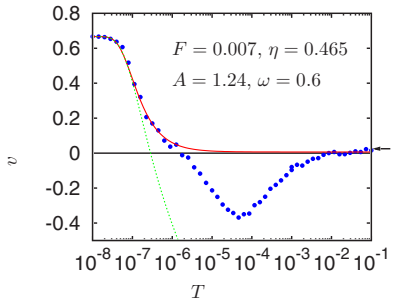

FIG. 15. (Color online) Same as Fig. 7, but for $F=0.007$. Lines: approximations (10) and (11) with $v_+=2/3$, $v_-=-1$, and $k_+=0.024\exp(-1.35\times 10^{-7}/T)$, $k_-=0.036$ (red solid line), $k_-=0.038-6.6\sqrt{T}$, $k_+=63\sqrt{T}\exp(-1.1\times 10^{-7}/T)$ (green dashed line).

asymptotic $v=(\tau/L)(F/\eta)\simeq 0.028$ according to Eq. (6) is approached. Therefore, the response behavior for the bias force around $F=0.007$ is as usual in the direction of F for low temperatures, but upon increasing the temperature first turns opposite to F, and then switches again to normal. Note that of the temperatures $T>0$ shown in Fig. 4 only the largest one falls into the ranges with positive v at $F\approx 0.007$.

VII. ABSOLUTE NEGATIVE CONDUCTANCE IN A JOSEPHSON JUNCTION

As a concrete experimental example of the predicted absolute negative mobility we consider the Stewart-McCumber or RCSJ (resistively and capacitively shunted junction) model [22,49] for the phase difference φ across a Josephson junction with capacity C, resistance R, critical current I_c (maximal Josephson current), and externally imposed current $I(t)$. Within this model, the φ dynamics is governed by the dimensionless equations (1) and (2) via the identifications

$$\varphi(t/\omega_p)=x(t),\quad I(t/\omega_p)=I_c[f(t)+F],$$

$$\eta=(RC\omega_p)^{-1},\quad T=C\,(\omega_p/I_c)^2k_BT^*, \tag{13}$$

where $\omega_p:=(2\pi I_c/\Phi_0 C)^{1/2}$ is the plasma frequency, $\Phi_0:=h/2e$ is the flux quantum, and k_BT^* is the thermal energy.

As far as the RCSJ model is concerned [22,49], the voltage $U(t)$ across the junction is given by $\Phi_0\dot{\varphi}(t)/2\pi$ (second Josephson relation) and hence its average according to Eqs. (3) and (13) by

$$\langle U\rangle=\frac{I_c}{C}\frac{\omega}{\omega_p^2}v. \tag{14}$$

Hence, absolute negative mobility for a Brownian particle (1) and (2) corresponds to absolute negative conductance in a Josephson junction, characterized by a dc component of the current $I(t)$ in Eq. (13) with sign opposite to the average voltage in Eq. (14).

Using the relations (13) and (14), our predictions from Fig. 4 can be realized by a Josephson junction with resistance $R\approx 0.2\ \Omega$, capacity $C\approx 250$ pF, critical current $I_c\approx 180\ \mu$A, temperature $T\approx 4.2$ K, driven by an ac current of frequency 28 GHz and amplitude 220 μA. The theoretically predicted I-V curve is shown in Fig. 16.

Additionally, by varying the ac amplitude, noisy I-V characteristics corresponding to bifurcation diagrams in the A direction should be accessible using the same junction. We remark that it is not necessary to hit the given parameters exactly as can be inferred from Fig. 6. Parameter values as exemplified in Fig. 16 are quite realistic and the resulting voltages $\langle U\rangle$ easily detectable.

Such an experiment [50] is presently under construction in the group of Dieter Kölle and Reinhold Kleiner in Tübingen (Germany). In fact, the effect might have already been implicitly observed (without further discussion or explanation) in the experimental work [51].

VIII. SUMMARY AND CONCLUSIONS

In conclusion, we have unraveled in Figs. 4, 14, and 15 three rather astonishing transport properties of the one-

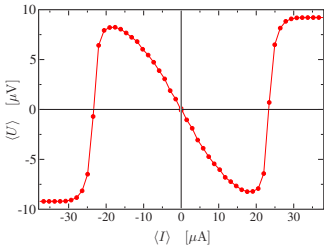

FIG. 16. (Color online) Same data as the green symbols in Fig. 4 but presented according to the Stewart-McCumber model (1), (2), (13), and (14) for a Josephson junction with resistance $R \approx 0.2\ \Omega$, capacity $C \approx 250$ pF, critical current $I_c \approx 180\ \mu$A, temperature $T \approx 4.2$ K, driven by an ac current of frequency 28 GHz and amplitude 220 μA.

dimensional stochastic dynamics (1) and (2): (i) a transport opposite to the static bias F (absolute negative mobility, Fig. 4), (ii) anomalous nonlinear response in the form of an average particle velocity that follows the direction of F for small F, but switches direction upon increasing F (Fig. 14), and (iii) a reversal of the transport direction from normal to anomalous at a fixed bias force F but for increasing temperature T (Fig. 15).

Apart from our own brief account [14] on such phenomena and the independent discovery of effect (i) by Machura *et al.* [15] (see Sec. V D), further preliminary hints to the existence of effects (i) and (ii) in a one-dimensional model (1), and an experimental trace of effect (i) are also implicitly contained already in the previously existing literature on Josephson junctions (see [34,48,51]). These findings are, however, not further discussed or explained in those works, because their focus is on other (dynamical) aspects of Josephson junctions. In fact, these "accidental" observations of the above effects (i),(ii) point to their remarkably common occurrence in dynamical systems like Eq. (1), as demonstrated by our present paper.

The above effects (i)–(iii) are observed for system parameters that are all of the order of magnitude of unity. This fact makes analytical studies extremely difficult; for instance, a perturbational approach becomes completely impossible. Accordingly, our detailed analysis of the model (1) and (2), its deterministic limit, and the effects of noise due to finite temperatures relies on extensive numerical simulations. An important exception is our strict proof using mathematical and physical arguments that the model (1) is minimal, in the sense that any of the terms in Eq. (1) are indispensable for the occurrence of the above phenomena.

Based on the numerical findings, we were able to develop a simple intuitive physical picture for the mechanism behind the observed response phenomena. Their occurrence is traced back to a subtle interplay of deterministic phase locked attractors, transient chaos on chaotic repellers, and noise-induced metastability of these dynamical "states." The latter has been shown to be well described by a simple rate-theoretical approach (see Sec. V A).

Apart from their fundamental interest [11,12,31] the effects (i)–(iii) may be applied for particle sorting [10], stabilization of unstable states, and making work (transport) available upon request [7]. For instance, one can see from Fig. 6 that particles with different friction coefficients (e.g., due to different sizes) can easily be guided into opposite directions by a suitable choice of the driving amplitude A.

As an experimental realization of the predicted effects we propose resistively and capacitively shunted Josephson junctions. Their dynamical behavior is characterized by the RCSJ or Stewart-McCumber model which is mathematically equivalent to our model (1) and (2). Suitable parameter values for which the above effects are predicted to occur are quite realistic experimentally.

Further experimental realization may be cold atoms in resonance with laser-induced optical lattices [52,53] and diffusion of single atoms and molecules on atomically clean crystal surfaces [54–56]. In such systems, the bias F and/or the driving $f(t)$ in Eq. (1) may also be substituted [57] by suitable "traveling-wave potentials" (pump) in place of the static $V(x)$. More precisely, $-V'(x(t))+f(t)+F$ in Eq. (1) is replaced by $-V'[x(t)-v_0t-g(t)]$, with average velocity v_0 and superimposed sinusoidal oscillations $g(t)$. Indeed, for the transformed variable $y(t) := x(t)-v_0t-g(t)$ one readily recovers [57] the original dynamics (1) with $F=-\eta v_0$ and a suitably chosen A in Eqs. (2). The effects predicted in the present work would result in averaged velocities that are considerably faster than the traveling velocity v_0 of the "entraining" potential, so that the particle is "running ahead" of the traveling-wave potential.

Finally, the basic physical mechanism as identified in our discussion of Figs. 1–3 is clearly quite robust against a large variety of modifications and generalizations of the dynamics (1) and (2). The only indispensable prerequisites are deterministic chaos, phase locking, and the symmetry properties $V(-x)=V(x)$ and $f(t+\tau/2)=-f(t)$. For example, we have found similar effects for various nonharmonic $V(x)$ and $f(t)$ in Eq. (1) and also when the "periodically rocking force field" $-V'(x)+f(t)$ in Eq. (1) is replaced by a "pulsating field" of the form $-V'(x)[1+f(t)]$.

ACKNOWLEDGMENTS

We thank T. Tél, D. Kölle, R. Kleiner, and P. Talkner for stimulating discussions. This work was supported by Deutsche Forschungsgemeinschaft under Grants No. SFB 613, No. RE 1344/3-1, and No. RE1344/5-1.

[1] For a review see T. Tél in *Directions in Chaos*, edited by Hao Bai-Lin (World Scientific, Singapore, 1990), Vol. 3.

[2] M. Franaszek, Phys. Rev. A **44**, 4065 (1991); P. Reimann, J. Stat. Phys. **82**, 1467 (1996).

[3] E. R. Kay, D. A. Leigh, and F. Zerbetto, Angew. Chem., Int. Ed. **46**, 72 (2007); P. Reimann, Phys. Rep. **361**, 57 (2002); H. Linke (special issue guest editor), Appl. Phys. A **75**, 167 (2002); J. Klafter and M. Urbakh (special issue guest editors), J. Phys.: Condens. Matter **17**, S3661 (2005).

[4] K. Wiesenfeld and F. Moss, Nature (London) **373**, 33 (1995); L. Gammaitoni, P. Hänggi, P. Jung, and F. Marchesoni, Rev. Mod. Phys. **70**, 223 (1998).

[5] Hu Gang, A. Daffertshofer, and H. Haken, Phys. Rev. Lett. **76**, 4874 (1996); G. Costantini and F. Marchesoni, Europhys. Lett. **48**, 491 (1999); P. Reimann, C. Van den Broeck, H. Linke, P. Hänggi, J. M. Rubi, and A. Pérez-Madrid, Phys. Rev. Lett. **87**, 010602 (2001).

[6] J. M. G. Vilar and J. M. Rubi, Phys. Rev. Lett. **86**, 950 (2001); Y. Seol, K. Visscher, and D. B. Walton, *ibid.* **93**, 160602 (2004).

[7] R. Eichhorn, P. Reimann, B. Cleuren, and C. Van den Broeck, Chaos **15**, 026113 (2005).

[8] R. Eichhorn, P. Reimann, and P. Hänggi, Phys. Rev. Lett. **88**, 190601 (2002); Phys. Rev. E **66**, 066132 (2002); B. Cleuren and C. Van den Broeck, *ibid.* **67**, 055101(R) (2003); R. Eichhorn and P. Reimann, Europhys. Lett. **69**, 517 (2005).

[9] B. Cleuren and C. Van den Broeck, Phys. Rev. E **65**, 030101(R) (2002); B. Jiménez de Cisneros, P. Reimann, and J. M. R. Parrondo, Europhys. Lett. **64**, 599 (2003).

[10] A. Ros, R. Eichhorn, J. Regtmeier, T. Duong, P. Reimann, and D. Anselmetti, Nature (London) **436**, 928 (2005); R. Eichhorn, A. Ros, J. Regtmeier, T. Duong, P. Reimann, and D. Anselmetti, Eur. Phys. J. Special Topics **143**, 159 (2007); J. Regtmeier, R. Eichhorn, T. Duong, P. Reimann, D. Anselmetti, and A. Ros, Eur. Phys. J. E **22**, 335 (2007); J. Regtmeier, S. Grauwin, R. Eichhorn, P. Reimann, D. Anselmetti, and A. Ros, J. Sep. Sci. **30**, 1461 (2007).

[11] T. J. Banis, I. V. Parshelyunas, and Y. K. Pozhela, Sov. Phys. Semicond. **5**, 1727 (1972).

[12] B. J. Keay, S. Zeuner, S. J. Allen, K. D. Maranowski, A. C. Gossard, U. Bhattacharya, and M. J. W. Rodwell, Phys. Rev. Lett. **75**, 4102 (1995).

[13] R. Eichhorn, P. Reimann, and P. Hänggi, Physica A **325**, 101 (2003); R. Eichhorn and P. Reimann, Phys. Rev. E **70**, 035106(R) (2004).

[14] D. Speer, R. Eichhorn, and P. Reimann, Europhys. Lett. **79**, 10005 (2007).

[15] L. Machura, M. Kostur, P. Talkner, J. Luczka, and P. Hänggi, Phys. Rev. Lett. **98**, 040601 (2007).

[16] H. Risken, *The Fokker-Planck Equation* (Springer, Berlin, 1984).

[17] M. Borromeo and F. Marchesoni, Phys. Rev. Lett. **84**, 203 (2000); P. Reimann, C. Van den Broeck, H. Linke, P. Hänggi, J. M. Rubi, and A. Pérez-Madrid, Phys. Rev. E **65**, 031104 (2002).

[18] E. G. Gwinn and R. M. Westervelt, Phys. Rev. Lett. **54**, 1613 (1985).

[19] M. Iansiti, Q. Hu, R. M. Westervelt, and M. Tinkham, Phys. Rev. Lett. **55**, 746 (1985).

[20] R. L. Kautz, J. Appl. Phys. **52**, 3528 (1981).

[21] R. L. Kautz and R. Monaco, J. Appl. Phys. **57**, 875 (1985).

[22] R. L. Kautz, Rep. Prog. Phys. **59**, 935 (1996).

[23] P. Jung, Phys. Rep. **234**, 175 (1993).

[24] Y. Yu and S. Han, Phys. Rev. Lett. **91**, 127003 (2003).

[25] F. Marchesoni, Phys. Lett. A **231**, 61 (1997).

[26] R. L. Kautz, Phys. Lett. A **125**, 315 (1987).

[27] P. Jung and P. Hänggi, Ber. Bunsenges. Phys. Chem. **95**, 311 (1991).

[28] M. Borromeo, G. Costantini, and F. Marchesoni, Phys. Rev. Lett. **82**, 2820 (1999).

[29] H.-J. Breymayer, Appl. Phys. A: Solids Surf. **33**, 1 (1984); P. Jung, J. G. Kissner, and P. Hänggi, Phys. Rev. Lett. **76**, 3436 (1996); J. L. Mateos, *ibid.* **84**, 258 (2000); J. L. Mateos, Acta Phys. Pol. B **32**, 307 (2001); J. L. Mateos, Physica A **325**, 92 (2003); M. Barbi and M. Salerno, Phys. Rev. E **62**, 1988 (2000); C. M. Arizmendi, F. Family, and A. L. Salas-Brito, *ibid.* **63**, 061104 (2001); M. Borromeo, G. Costantini, and F. Marchesoni, *ibid.* **65**, 041110 (2002); W. S. Son, I. Kim, Y. J. Park, and C. M. Kim, *ibid.* **68**, 067201 (2003); F. Marchesoni, S. Savel'ev, and F. Nori, *ibid.* **73**, 021102 (2006); M. Kostur, L. Machura, P. Hänggi, J. Luczka, and P. Talkner, Physica A **371**, 20 (2006).

[30] H. Schanz, T. Dittrich, and R. Ketzmerick, Phys. Rev. E **71**, 026228 (2005); S. Denisov, S. Flach, and P. Hänggi, Europhys. Lett. **74**, 588 (2006).

[31] R. K. P. Zia, E. L. Praestgaard, and O. G. Mouritsen, Am. J. Phys. **70**, 384 (2002).

[32] We remark that g and h containing δ spikes or a shot noise $\xi(t)$ would lead to discontinuous $x(t)$ and hence spoil the argument.

[33] G. A. Cecchi and M. O. Magnasco, Phys. Rev. Lett. **76**, 1968 (1996).

[34] A first hint along this line is implicitly buried in three papers by Kautz, namely, in Fig. 4 of [20], Fig. 3(a) of [21], and Figs. 13(c) and 25(b) of [22]. A second hint comes from the recent works [30] on the Hamiltonian limit $\eta \to 0$ in Eq. (1), implying the existence of deterministic solutions running against the force F for suitably chosen initial conditions. Investigating and optimizing their stability against dissipation and noise (finite η) could have been an alternative starting point of our present work, but in fact our approach was different.

[35] C. C. Chi and C. Vanneste, Phys. Rev. B **42**, 9875 (1990).

[36] We use the term "attractor" both for a stable, "attracting" orbit $x(t)$ of the dynamics and for the thereby sampled "attracting set" in phase space. In the latter case we tacitly consider the reduced version of the spatially periodic dynamics (1), i.e., x and $x+L$ are identified as far as the attracting set is concerned.

[37] Such a solution may be either chaotic or of nonchaotic, aperiodic type (Feigenbaum attractor).

[38] Such a solution may be either chaotic or quasiperiodic. The former case is closely related with deterministic diffusion [58]. The latter case is possible only for finite bias F for the specific deterministic dynamics (1) and (2) (see Sec. V in [22]).

[39] Other phase locked attractors (with different velocities), which have not been found by our numerical method due to the finite grid resolution in η and A and the limited number of random initial conditions sampled, either have very small basins of attraction and/or exist only in very small regions of the (η, A) parameter space. The same applies for non phase locked attractors that may coexist with phase locked attractors in the considered parameter region.

[40] For $M=T=0$ in Eq. (1), the velocity (3) must be unique (see [59] and Sec. 5.3.2 in [3(b)]), though one may still have coexisting attractors [60].
[41] C. Grebogi, E. Ott, and J. A. Yorke, Phys. Rev. Lett. **48**, 1507 (1982); R. L. Kautz, J. Appl. Phys. **62**, 198 (1987).
[42] F. T. Arecchi, R. Badii, and A. Politi, Phys. Rev. A **32**, 402 (1985); R. L. Kautz, J. Appl. Phys. **58**, 424 (1985); P. Reimann, R. Müller, and P. Talkner, Phys. Rev. E **49**, 3670 (1994).
[43] For $T>0$ and $F=0$ one always has $v=0$ due to symmetry and ergodicity.
[44] In the sense that points located exactly on an unstable trajectory have measure zero, and that the basins of attraction of possibly coexisting attractors have negligible measure (see remark [39]).
[45] This implicitly assumes that the escape rate is independent of the initial condition in the synchronous basin of attraction, which is well justified for small temperatures. Regions of the synchronous basin of attraction close to its borders or very far from the attractor, which might lead to a different escape rate have small statistical weights and can be neglected.
[46] J. Lehmann, P. Reimann, and P. Hänggi, Phys. Rev. Lett. **84**, 1639 (2000); Phys. Rev. E **62**, 6282 (2000).
[47] J. C. Sommerer, Phys. Lett. A **176**, 85 (1993).
[48] A first theoretical hint for the occurrence of this effect in the closely related Stewart-McCumber model for Josephson junctions (see Sec. VII) has been observed in Fig. 8 of [61], however, without any further discussion or explanation.
[49] W. C. Steward, Appl. Phys. Lett. **12**, 277 (1968); D. E. McCumber, J. Appl. Phys. **39**, 3113 (1968); K. K. Likharev, *Dynamics of Josephson Junctions and Circuits* (Gordon and Breach, Philadelphia, 1986); W. Buckel and R. Kleiner, *Superconductivity: Fundamentals and Applications* (Wiley-VHC, Berlin, 2004).
[50] A. Sterck, R. Kleiner, and D. Koelle, Phys. Rev. Lett. **95**, 177006 (2005); M. Beck, E. Goldobin, M. Neuhaus, M. Siegel, R. Kleiner, and D. Koelle, *ibid.* **95**, 090603 (2005).
[51] N. F. Pedersen, O. H. Soerensen, B. Dueholm, and J. Mygind, J. Low Temp. Phys. **38**, 1 (1980).
[52] G. Grynberg and C. Robilliard, Phys. Rep. **355**, 335 (2001).
[53] R. Gommers, S. Bergamini, and F. Renzoni, Phys. Rev. Lett. **95**, 073003 (2005).
[54] T. Ala-Nissila, R. Ferrando, and S. C. Ying, Adv. Phys. **51**, 949 (2002).
[55] M. Azzouz, H. J. Kreuzer, and M. R. A. Shegelski, Phys. Rev. B **66**, 125403 (2002).
[56] G. Antczak and G. Ehrlich, Phys. Rev. B **71**, 115422 (2005).
[57] M. Borromeo and F. Marchesoni, Phys. Lett. A **249**, 199 (1998); C. Van den Broeck, Europhys. Lett. **46**, 1 (1999); R. Landauer and M. Büttiker, Phys. Scr. **T9**, 155 (1985); L. P. Faucheux, G. Stolovitzky, and A. Libchaber, Phys. Rev. E **51**, 5239 (1995); V. I. Talyanskii, J. M. Shilton, M. Pepper, C. G. Smith, C. J. B. Ford, E. H. Linfield, D. A. Ritchie, and G. A. C. Jones, Phys. Rev. B **56**, 15180 (1997); C. Rocke, S. Zimmermann, A. Wixforth, J. P. Kotthaus, G. Böhm, and G. Weimann, Phys. Rev. Lett. **78**, 4099 (1997).
[58] H. Fujisaka and S. Grossmann, Z. Phys. B: Condens. Matter **48**, 261 (1982); T. Geisel and J. Nierwetberg, Phys. Rev. Lett. **48**, 7 (1982); M. Schell, S. Fraser, and R. Kapral, Phys. Rev. A **26**, 504 (1982).
[59] A. Ajdari, D. Mukamel, L. Peliti, and J. Prost, J. Phys. I **4**, 1551 (1994).
[60] R. Bartussek, P. Hänggi, and J. G. Kissner, Europhys. Lett. **28**, 459 (1994).
[61] D. C. Cronemeyer, C. C. Chi, A. Davidson, and N. F. Pedersen, Phys. Rev. B **31**, 2667 (1985).